Journal of Quantitative Spectroscopy & Radiative Transfer ▮ (▮▮▮▮) ▮▮▮–▮▮▮

Contents lists available at ScienceDirect

Journal of Quantitative Spectroscopy & Radiative Transfer

journal homepage: www.elsevier.com/locate/jqsrt

Does variation in mineral composition alter the short-wave light scattering properties of desert dust aerosol?

Andrew J.A. Smith *, Roy G. Grainger

Atmospheric, Oceanic and Planetary Physics, University of Oxford, Clarendon Laboratory, Parks Road, Oxford OX1 3PU, UK

ARTICLE INFO

Article history:
Received 15 April 2013
Received in revised form
5 August 2013
Accepted 6 August 2013

Keywords:
Mineral dust
Aerosol refractive index
Refractive index variability
Aerosol remote sensing
Radiative transfer

ABSTRACT

Mineral dust aerosol is a major component of natural airborne particulates. Using satellite measurements from the visible and near-infrared, there is insufficient information to retrieve a full microphysical and chemical description of an aerosol distribution. As such, refractive index is one of many parameters that must be implicitly assumed in order to obtain an optical depth retrieval. This is essentially a proxy for the dust mineralogy.

Using a global soil map, it is shown that as long as a reasonable refractive index for dust is assumed, global dust variability is unlikely to cause significant variation in the optical properties of a dust aerosol distribution in the short-wave, and so should not greatly affect retrievals of mineral dust aerosol from space by visible and near-infrared radiometers. Errors in aerosol optical depth due to this variation are expected to be $\lesssim 1\%$. The work is framed around the ORAC AATSR aerosol retrieval, but is equally applicable to similar satellite retrievals. In this case, variations in the top-of-atmosphere reflectance caused by mineral variation are within the noise limits of the instrument.

1. Introduction

1.1. Mineral dust

While not as prevalent in the global atmosphere as maritime aerosol, local dust events dominate total aerosol optical depth in deserts and the surrounding regions during periods of high wind. Long range transport of desert dust (particularly the smaller particles) means that the dust can be seen all over the world, with deposition over the Atlantic and in the Amazon basin being well known occurrences [1]. Saharan mineral dust is thought to play a vital role in the support of vegetation in the Amazon basin and provides nutrient iron to the biogeochemical cycle of the ocean systems [2]. Saudi Arabian dust outbreaks have been linked to weakening of the monsoon trough over India [3].

Mineral dust aerosol is naturally occurring, although desertification caused by changes to climate and to land use (e.g. [4,5]) may be responsible for changes in emission patterns and quantities. Dust is injected into the atmosphere by saltation: a jumping motion whereby already detached, larger particles collide with obstructions on the surface bed, projecting smaller particles into the air [6] (wind alone does not have sufficient energy to remove particles from the surface bed). Since fine mineral dust (light enough to be lofted) is quickly removed from the surface, most of a desert region is not a significant dust source. This means that in the majority of desert regions, surface mineral dust is very coarse. Specific areas such as the Bodélé Depression in Chad, the world's largest dust source [7], have favourable conditions that include strong surface winds, optimum topography, and annual deposition of mineral dust.

Sand composition determines the refractive index (RI), with increasing hematite content leading to increased short-wave absorption (and sand with a more reddish hue) [8]. As such, one would suspect that across the world

* Corresponding author. Tel.: +44 1865 272915; fax: +44 1865 272923.
E-mail address: smith@atm.ox.ac.uk (A.J.A. Smith).

0022-4073/$ - see front matter © 2013 Elsevier Ltd. All rights reserved.
http://dx.doi.org/10.1016/j.jqsrt.2013.08.005

(and indeed within particular regions), variation in the mineralogy of mineral dust and, by extension, in the mineralogy of dust aerosol, would be significant. It would then be expected that the RI of the mineral dust aerosol would vary. Whether or not this causes unacceptable errors in calculations of optical properties is the next question.

Fig. 1 shows how several datasets of mineral dust RI compare in the short-wave. Models have real parts of RI in the visible that range from $n=1.48 \rightarrow 1.56$ with a median value of $n=1.53$. Absorption values can vary by almost an order of magnitude. It is likely that the dust sources used to estimate these values are different.

1.2. Satellite aerosol retrievals in the short-wave

Satellite instruments such as (A)ATSR [14], AVHRR [15], MISR [16], MODIS [17], and SEVIRI [18] are radiometers, using specifically chosen wavelengths with relatively narrow spectral bandwidths. For aerosol detection, the channels generally used are around 550 nm, 860 nm, and 1.6 μm since here the size of the aerosols is similar to the wavelength of the measured light, and we are within atmospheric window regions where there is minimal interference from molecular scattering and absorption (a list of available wavelengths is given in Table 1). However, the measurements are inherently under-constrained, no matter how much of the shortwave spectrum is sampled, and as such retrieval methods must make assumptions about the type of aerosol being observed,

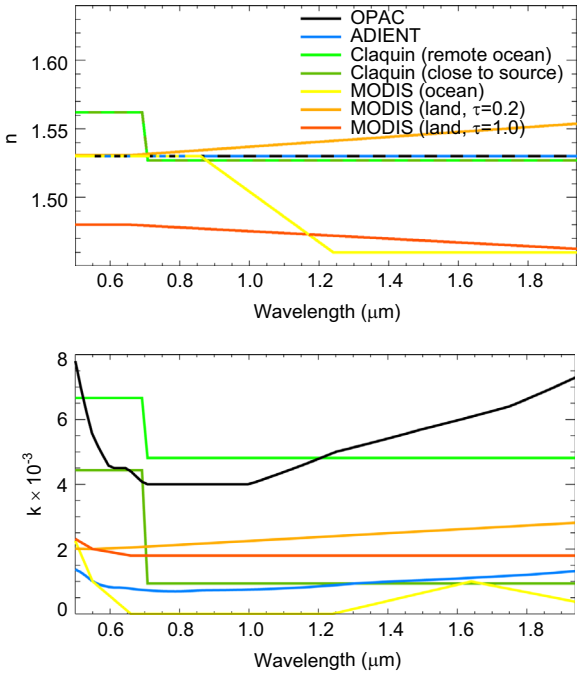

Fig. 1. The real (n) and imaginary (k) parts of desert dust refractive indices as used, or recommended by various science teams. Datasets are: The Optical Properties of Aerosols and Clouds (OPAC) dataset [9]; a literature review of reported aerosol RI to the ADIENT consortium [10]; Claquin et al. [11]; and those used by the MODIS team over ocean [12] and over land (where RI is dependent on the optical depth, τ) [13].

Table 1
Various channels used by broadband radiometers which measure aerosol properties in the visible and NIR. The centres of each channel are given, so (particularly in the case of MODIS) channels can overlap.

Satellite	Channels (μm)
(A)ATSR	0.55, 0.66, 0.87, 1.6, 3.7, 10.8, 12.0
AVHRR	0.63, 0.86, 1.6, 3.7, 10.8, 12.0
MISR	0.45, 0.58, 0.67, 0.87
MODIS	0.41, 0.44, 0.47, 0.48, 0.53, 0.55, 0.56, 0.64, 0.66, 0.67, 0.74, 0.86, 0.87, 0.90, 0.93, 0.94, 1.2, 1.4, 1.6, 2.1, 3.7, 3.9, 4.0, 4.4, 4.5, 6.7, 7.3, 8.6, 9.7, 11.0, 12.0, 13.3, 13.6, 13.9, 14.2
SEVIRI	0.6, 0.8, 1.6, 3.9, 6.2, 7.3, 8.7, 9.7, 10.8, 12.0, 13.4

the mixing between different types, the sizes of these types, and their composition.

2. Method

In order to investigate whether variation in desert dust composition is an important factor in determining dust light scattering properties, a picture of global mineral dust RI and its likelihood of atmospheric injection was built up. This could then be used to create a weighted distribution of RI values which are used with a sensible dust size distribution to obtain dust extinction, optical depth, and phase function.

The Earth was divided into gridboxes. Obtaining the mean RI for each selected gridbox is a three step process. First, an approximate soil composition is obtained on a regular grid over the whole Earth, built of common minerals. Next, the RI values of the individual minerals are combined for each soil type, giving a picture of how RI varies geographically. Finally, the world-wide spread is reduced to a histogram of RI values. These are weighted using a simple emissions model so that only areas where dust is likely to be lofted into the atmosphere contribute to the average.

2.1. FAO/UNESCO Digital Soil Map of the World

The FAO/UNESCO Digital Soil Map of the World [19] is a regularly gridded $5' \times 5'$ resolution global map, with each cell containing a mix of soil types. This is equivalent to a resolution of ~ 9 km $\times$ 9 km at the equator, and ~ 8 km $\times$ 9 km at the Bodélé depression, Sahara's largest source of lofted dust [20], with an approximate area of 150 km $\times$ 150 km [21]. Using a similar method to Nickovic et al. [22], a list of FAO soil types found in arid areas [23, Table 2] was used. This contains the normalised composition by weight of important dust minerals: in this case illite, kaolinite, smectite, calcite, quartz, felspath (or felspar), gypsum and hematite. The minerals are divided into those found in clay fraction (<2 μm) and the larger silt fraction ($2 \rightarrow 50$ μm). There is an even larger, sand fraction ($50 \rightarrow 200$ μm), but these particles are too large to be lofted for extended periods so were not included in calculations. The FAO soil 'textures' (coarse, medium or fine) were converted to soil sizes using conversions to dry sieving sizes from Laurent et al. [24, Table 4]. For each $5' \times 5'$ area of land, the FAO map gives up to 8 soil types which make a proportion

Please cite this article as: Smith AJA; Grainger RG. Does variation in mineral composition alter the short-wave light scattering properties of desert dust aerosol? J Quant Spectrosc Radiat Transfer (2013), http://dx.doi.org/10.1016/j.jqsrt.2013.08.005

of the land area, each with its own soil texture. Of course, not all of these soils will be suitable for lofting into the air.

2.2. Converting soil types into refractive indices

All soil types not given in the previously mentioned mineralogical breakdown of mineral dust soils [23] were defined as non-arid and ignored in subsequent calculations. Weighting the RI of each mineral, using the appropriate clay and silt fractions for each soil type, the bulk refractive index of each soil type could be obtained by combination of individual minerals using the Bruggeman formula (e.g. [25]). This relates a bulk effective permittivity, ϵ_{eff}, to the various component phases with permittivities, ϵ_i, and volume fractions, v_i:

$$\sum_i v_i \frac{\epsilon_i - \epsilon_{\text{eff}}}{\epsilon_i + 2\epsilon_{\text{eff}}} = 0. \quad (1)$$

Refractive index values in the visible and near-infrared were obtained for the minerals mentioned above. Illite, kaolinite, felspar and montmorillonite data were obtained from Egan and Hilgeman [26], hematite and quartz from Jacquinet-Husson et al. [27], calcite from Ghosh [28], and gypsum from Roush et al. [29]. Calcite values were assumed non-absorbing ($k=0$). These values are shown in Fig. 2. Here we see why hematite content is such an important determining factor in the appearance of sand, particularly in the visible. The negative gradient in k will lead to more scattering at the longer wavelengths, hence the red hue is given to sands with greater hematite content.

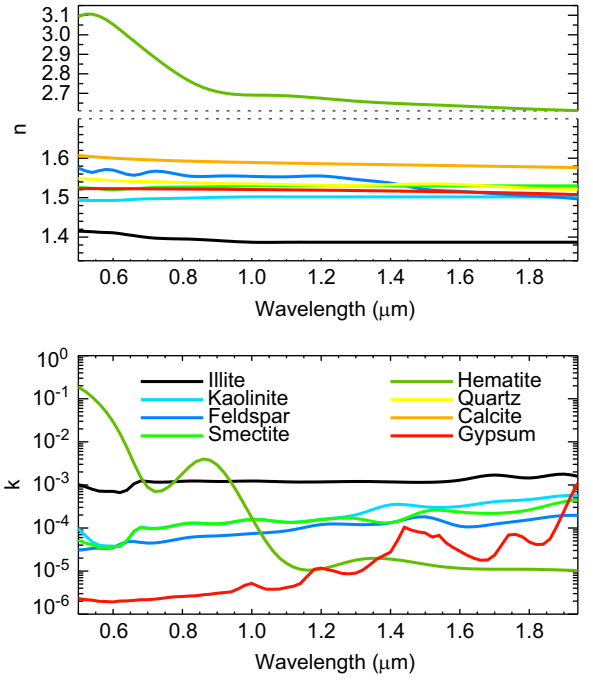

Fig. 2. The real (n) and imaginary (k) parts of the principal mineralogical components of desert dust aerosol. Illite, kaolinite, feldspar, and smectite data are from Egan and Hilgeman [26]. Hematite and quartz are from the GEISA database [27]. Calcite and gypsum are from Ghosh [28] and Roush et al. [29] respectively. Note that the axis for n has a discontinuity so that hematite can be included. Quartz and calcite do not absorb at these short wavelengths, so do not appear on the k plots.

2.2.1. Birefringence

Quartz, calcite, and hematite are birefringent, meaning that their refractive indices vary with the orientation of their crystal lattice (e.g. [30, Section 8.4]). Light propagating in a general direction through these crystals will encounter an asymmetric arrangement of atoms. Furthermore, all three minerals have a trigonal structure (i.e. an axis of three-fold rotational symmetry), so that there is one direction for propagating light in which atoms are arranged symmetrically, known as the optical axis. This leads to two speeds with which wavelets of light can travel through the medium: the ordinary-, or o-waves travel perpendicular to the optical axis with a speed c/n_o, while the extraordinary-, or e-waves, travel parallel with a speed c/n_e. Here, c is the speed of light in a vacuum and n_o and n_e are the ordinary and extraordinary refractive index values. Since it is assumed that any sand particles observed are randomly orientated, o-wave and e-wave values of n and k are combined, with twice the weighting for the o-rays since there are two directions that are perpendicular to the optical axis and only one direction parallel to it.

2.3. Weighting by likelihood of emission

The weighting used a basic scheme depending on the clay fraction of the mineral dust in a grid box, and a measure of peak wind speed at the same position, based on a simplification of saltation flux calculations. The vertical emission flux of fine particles, F, is linearly related to the saltation flux, G (the flux of particles travelling parallel to the soil surface), by the sand blasting efficiency, α, so that

$$F = \alpha G. \quad (2)$$

An empirical relation can be used to derive α [24]

$$\alpha = 10^{(0.134 \times \%\text{age clay} - 6)}, \quad (3)$$

and the full saltation flux calculation [31] was simplified to

$$G \propto u_{peak}^3, \quad (4)$$

where u_{peak} is the peak wind speed 10 m above the surface, and we have assumed a constant surface roughness and particle fluxes independent of particle size.

Peak horizontal wind speed was obtained from a year's worth of ECMWF operational analysis data (April 2006–March 2007). The horizontal wind speed mean and standard deviation were calculated, and peak wind speed was defined as two standard deviations above the mean wind speed for each location. At the Bodélé depression, this leads to a peak wind speed of 11.9 m s^{-1}, which is in good agreement with measured wind speed during dust storms of 13 ± 1 m s^{-1} given by Koren and Kaufman [32].

Although not taken into account in this study, higher wind speeds cause larger aerosols to be preferentially

Please cite this article as: Smith AJA; Grainger RG. Does variation in mineral composition alter the short-wave light scattering properties of desert dust aerosol? J Quant Spectrosc Radiat Transfer (2013), http://dx.doi.org/10.1016/j.jqsrt.2013.08.005

released into the atmosphere [33]. Since our final mineral compositions are size independent, and the atmospheric size distribution of the dust is prescribed (as defined below), it was not considered necessary to complicate the emissions scheme in this manner.

Finally, the presence of vegetation all but completely inhibits emission of mineral dust. Areas of vegetation can be estimated using normalised difference vegetation index, $\mathrm{NDVI} = (R_{\mathrm{nIR}} - R_{\mathrm{red}})/(R_{\mathrm{nIR}} + R_{\mathrm{red}})$, where R_{nIR} and R_{red} are the reflectances in the near-infrared and red regions respectively. Using AATSR ORAC monthly-mean atmospheric-aerosol-corrected NDVI for March 2004 [34], a threshold of $\mathrm{NDVI} < 0.08$ was used. Above this value suggests a vegetation cover dense enough to prevent atmospheric injection [35], and so emission was not permitted in such regions. This threshold was selected *ad hoc* by observation of the regions that would be included with various values of cut-off. At the threshold values, there is an abrupt change from no emission to full emission.

Fig. 3 shows the output values produced at various steps in the method. Comparisons of the approximate emissions model (shown in the final panel) with a far more detailed calculation for the Saharan region [24] have good agreement. Major known sources, for example along the West Saharan coast, in central Algeria (27°N, 2°W), and the Bodélé depression in Chad (17°55′N, 19°7′E) are well represented, however this simple model predicts a few emissions which are completely absent from the full calculation (for example, along the banks of the Red Sea). The most likely reason for this would be soil moisture,

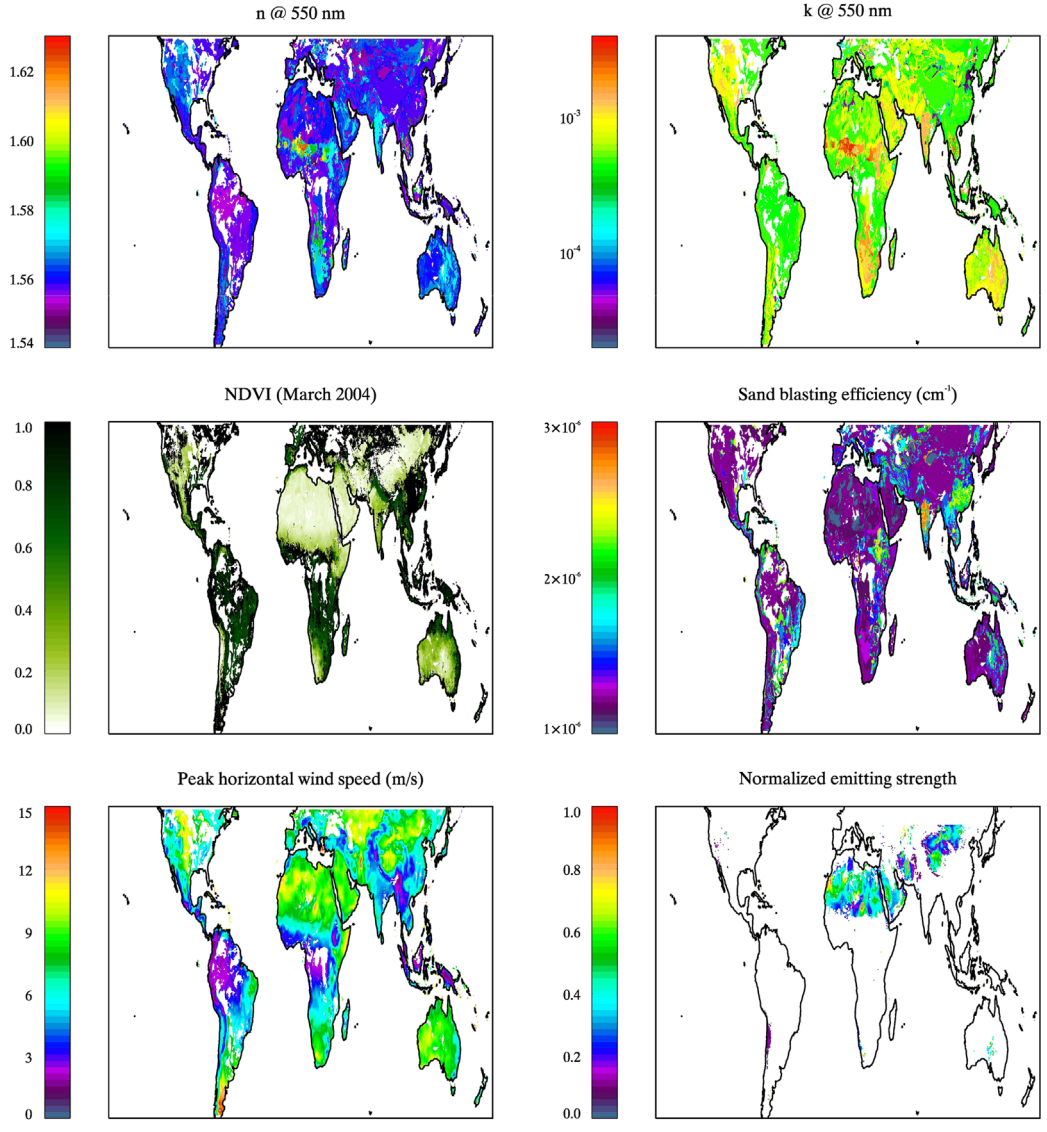

Fig. 3. The soil refractive index for arid soil types over the Earth's surface is shown, followed by the various parameters required to calculate the relative emitting strength of an area of the world. NDVI data are the monthly mean from March 2004 AATSR data. An area is only allowed to emit if its NDVI value is less than 0.08. Sand blasting efficiency, α, is only calculated for the soil types which are mineral dust as defined by Claquin et al. [23] and is obtained as a function of the clay fraction, using Eq. (3). Peak horizontal wind speed is from ECMWF reanalysis data. The final result, normalised emitting strength, is a function of the previous plots.

Please cite this article as: Smith AJA; Grainger RG. Does variation in mineral composition alter the short-wave light scattering properties of desert dust aerosol? J Quant Spectrosc Radiat Transfer (2013), http://dx.doi.org/10.1016/j.jqsrt.2013.08.005

which strongly restricts emission [36], but is not accounted for in this scheme.

2.4. Calculating aerosol optical properties

Aerosol optical properties are calculated using the microphysical model developed for the Oxford-RAL Aerosol and Cloud retrieval scheme [37], which can currently process data from the (A)ATSR, SEVIRI, and MODIS instruments. The retrieval has two output aerosol properties: the aerosol optical depth at 550 nm (τ_{550}); and the aerosol effective radius (r_{eff}). The effective radius is defined as

$$r_{\text{eff}} = \frac{\int_0^\infty r^3 n(r)\, dr}{\int_0^\infty r^2 n(r)\, dr}, \tag{5}$$

where $n(r)$ is the number distribution of aerosol radii.

2.4.1. The desert dust microphysical model

The mineral dust aerosol microphysical model is based on the "Desert" aerosol class given in the OPAC package [9]. In this, there are four aerosol lognormal number distributions as a function of particle radius with properties given in Table 2.

The water soluble mode represents the ubiquitous background aerosol formed from gas-to-particle conversion. In order to vary r_{eff}, the relative mixing of the four modes is altered, while in order to vary τ_{550}, the total number concentration of the aerosol is altered.

Based on SEM and TEM electron microscopy measurements of mineral dust aerosol, reported characteristics are rough edged, non-spherical particles with the majority of aspect ratios (*AR*, the ratio between maximum length and width) of $\sim 1.3 \rightarrow 2.2$ [38–43] although the larger particles can become more elongated [40]. However, studies attempting to reproduce dust's IR spectroscopy [44,43,45], polarimetric effects [46,45], or the full phase function in the visible (particularly) backward-scattering effects [46,47] have required a significant number of accumulation mode dust particles with much larger *AR* values, likely due to the clay particles in the accumulation mode being "flakes", best represented by "highly eccentric oblate spheroids" [45]. Distributions of shape have included uniform ($n(AR) = \text{constant}$) [46], cubic ($n(AR) \propto |AR-1|^3$) [47] and modified lognormal (described below) [41].

Differences between the extreme *AR* required in the IR and the moderate distributions of *AR* required in the analysis of electron microscope images is likely due to the size of particles preferentially sampled by the techniques as well as the orientation of flake-like particles relative to the viewing direction in SEM analysis. The computational overhead on light scattering calculations with very high aspect ratios is extreme, and available look-up tables spheroid calculations [48] are limited to $AR \leq 3$. As such, the desert dust aerosol modes were modelled as spheroids, with a modified lognormal distribution of aspect ratios as given by Kandler et al. [41]:

$$n(AR) = \frac{1}{\sqrt{2\pi}\xi(AR-1)} \times \exp\left[-\frac{1}{2}\left(\frac{\ln(AR-1)-\mu}{\xi}\right)^2\right], \tag{6}$$

where $\xi = 0.6579$ and $\mu = -0.4502$ giving a median aspect ratio $AR_{median} = 1.66$. Variation in the aspect ratio as a function of mineralogy and size was reported by Kandler et al. [41] and Meland et al. [45], but this was not included in these calculations as it would have led to an unfeasibly large number of light scattering calculations.

Table 2
The OPAC desert dust size distribution. Mass mixing ratio (MMR), lognormal median radius (r_m), spread (S), and effective radius (r_{eff}) are shown. Radius values are reported in μm. Each aerosol mode has prescribed refractive index which (with the exception of the water soluble mode) was ignored in this study.

Aerosol mode	MMR (%)	r_{m}	S	r_{eff}
Water soluble	1.8	0.26	2.24	0.133
Dust nucleation	3.3	0.07	1.95	0.213
Dust accumulation	74.7	0.39	2.00	1.30
Dust coarse	20.2	1.90	2.15	8.22
Full distribution				1.62

2.4.2. The desert dust optical properties

The overall optical depth at wavelength λ,

$$\tau(\lambda) = \int_0^\infty \beta^{\text{ext}}(z,\lambda)\, dz, \tag{7}$$

is controlled by the total number concentration, and the effective radius by the relative mixing of the different distributions, such that the extinction is

$$\beta^{\text{ext}}(z,\lambda) = \sum_i \int_0^\infty N_i(r,z)\sigma_{\text{ext}}(r,\lambda,RI_i(\lambda))\, dr, \tag{8}$$

here σ_{ext} is the aerosol extinction cross-section, N_i is the number density distribution at radius r and altitude z, and the index i represents an aerosol mode such as those given in Table 2. Aerosol distribution light scattering properties were obtained using the look-up tables of spheroid optical properties by Dubovik et al. [48]. The range of aspect ratios provided was $1 < AR < 3$. In these tables, particles with very low absorption ($k < 5 \times 10^{-4}$) were considered to be at the lower limit of absorption, and so all values of k below this were set to this value. Comparisons of light scattering properties for spherical particles with all other properties the same showed that this approximation was appropriate, leading to errors at least 5 times smaller than changes due to increasing absorption.

3. Results

Fig. 4 shows final calculations for the expected refractive index at the point of emission. Noticeable emitting regions are the Sahara, the Namib desert, central Asia, central Australia, Nevada and the Chilean coast. The calculations are shown for $\lambda = 550$ nm but results are very similar throughout the visible and NIR. Each grid point has a different relative emission rate (see Fig. 3) which is used to create the weighted histograms.

The mean value of $n_{550} \simeq 1.56$ (with standard deviation of 0.006) is at the higher end of previous studies [10, 49–51] which have a range of reported values of $n = 1.53 \rightarrow 1.56$. The absorbing (imaginary) part centring around $k_{550} \leq 10^{-3}$ ($\bar{k} = 6.2 \times 10^{-4}$ with standard deviation of 2.7×10^{-4}) is slightly less than other studies

Please cite this article as: Smith AJA; Grainger RG. Does variation in mineral composition alter the short-wave light scattering properties of desert dust aerosol? J Quant Spectrosc Radiat Transfer (2013), http://dx.doi.org/10.1016/j.jqsrt.2013.08.005

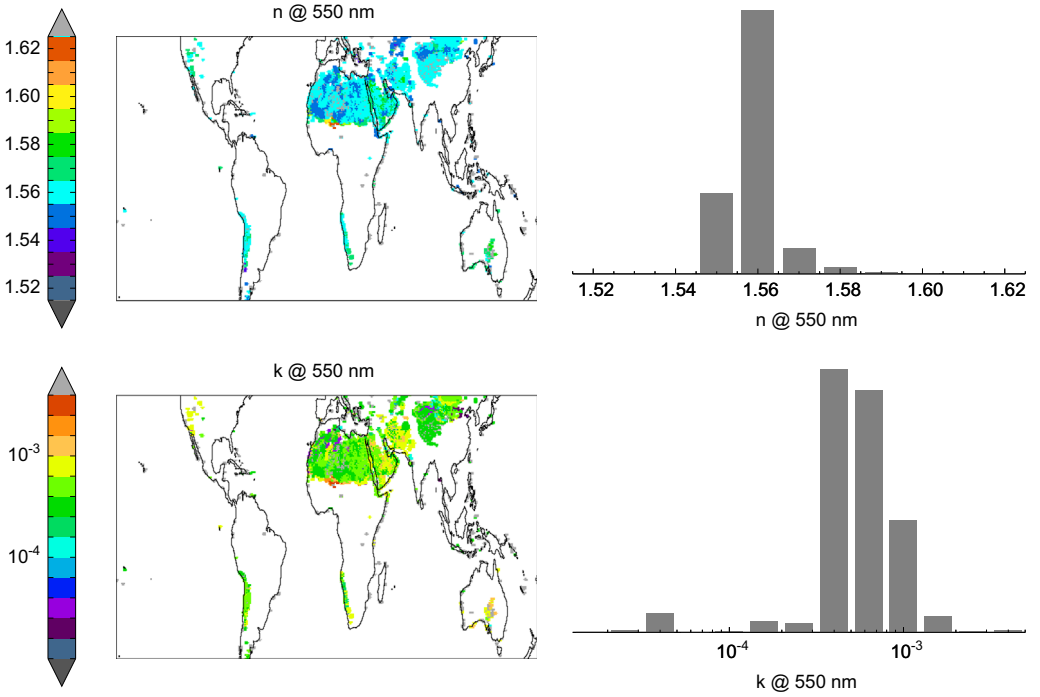

Fig. 4. Showing the spread of the real and imaginary parts of mineral dust aerosol refractive index at $\lambda = 550$ nm for weighted global dust emissions. Histograms are weighted by the normalized emitting strength shown in Fig. 3.

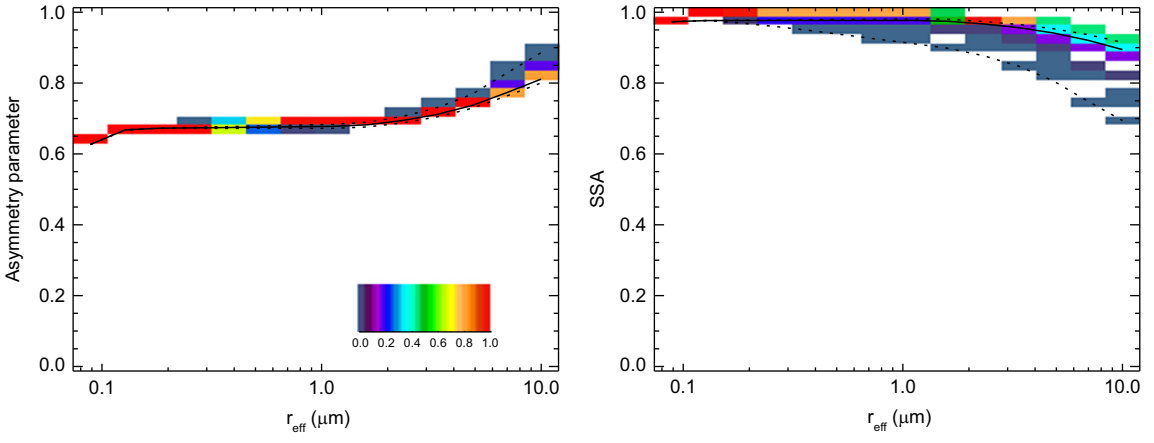

Fig. 5. Showing the spread of optical properties from the mean value at 550 nm, using the weighted spread of RI from the histograms in Fig. 4. The solid line is the overall averaged scattering. The colours show the density of points within a grid box (so that vertically summing the boxes results in unity). Dashed lines are the extreme values given by the range of n and k. (For interpretation of the references to colour in this figure caption, the reader is referred to the web version of this article.)

(which range from 5×10^{-4} [51] to 1.5×10^{-3} [50]) and far less absorbing than OPAC values which are thought to be too large [10]. Identical calculations at 660, 870, 1600 nm had extremely similar results.

Further inspection shows that areas with high levels of hematite (which has $n_{550} = 3.1$) have the largest (real and imaginary) refractive indices, such as the Sahel region which is known to have minerals with higher proportions of iron oxides [23,52]. Inaccuracies created by such a large number of assumptions about the soil making up our lofted dust (e.g. mapping FAO textural classes to soil types; the use of data with a low number of sampling points to generate the mineral fractions given by Claquin et al. [23]; no account taken of atmospheric processing of the mineral dust [53]) are bound to lead to errors in the calculations of mineral RI, but it is still reasonable that the spread of values could be a useful indicator of the importance of RI in aerosol light scattering calculations for desert dust.

Using the histograms of RI spread as shown in Fig. 4, one can calculate the optical properties of an aerosol distribution with this amount of mineralogical variation, using the method described in Section 2.4. This is shown for $\lambda = 550$ nm in Fig. 5, in which the spread of the asymmetry (or anisotropy) parameter and the single

Please cite this article as: Smith AJA; Grainger RG. Does variation in mineral composition alter the short-wave light scattering properties of desert dust aerosol? J Quant Spectrosc Radiat Transfer (2013), http://dx.doi.org/10.1016/j.jqsrt.2013.08.005

Table 3
The effect of varying mineralogy on the optical properties of a full mineral dust aerosol class. The relative variances (RV) quoted are the standard deviations (SD) divided by the mean. These calculations are for $r_{\text{eff}} = 1.62$ μm.

λ (μm)	$\beta^{\text{ext}} \times 10^{-5}$ (km^{-1})			Asymmetry parameter			$\tilde{\omega}_0$			$P(180^\circ)$		
	Mean	SD	RV (%)	Mean	SD	RV (%)	Mean	SD	RV (%)	Mean	SD	RV (%)
0.55	6.558	0.005	0.08	0.683	0.002	0.31	0.974	0.008	0.85	0.655	0.010	1.54
0.66	6.420	0.005	0.07	0.675	0.002	0.31	0.977	0.008	0.77	0.653	0.010	1.59
0.86	6.258	0.005	0.09	0.668	0.002	0.34	0.980	0.006	0.66	0.626	0.011	1.71
1.59	5.786	0.018	0.31	0.665	0.003	0.43	0.987	0.004	0.44	0.500	0.009	1.85

scatter albedo, $\tilde{\omega}_0$, is given. The asymmetry parameter is a measure of how much the light is forward- (or backward-) scattered and so a good low-order representation of the phase function (the full angular description of the redistribution of energy by the scattering body). The single scatter albedo is the ratio of scattered light to total scattered and absorbed light. The plot of extinction coefficient, β^{ext}, was omitted due to the narrowness of its spread. At a reasonable effective radius of $r_{\text{eff}} = 1.62$ μm, the relative variation (standard deviation divided by mean) of β^{ext}, the asymmetry parameter, and $\tilde{\omega}_0$ are 0.1%, 0.3%, and 0.9% respectively as shown in Table 3. The variation in the amount of backscattered light, $P(180^\circ)$, can be as large as 2%.

Almost all of this variation is caused by the imaginary part of RI. Holding n constant while varying k yields very similar results to allowing the full range of both n and k. Conversely, holding k constant while allowing n to vary reduces greatly the variation in optical properties seen.

Finally, to characterise how the variation in optical properties would affect the measured radiances, these varied optical properties were fed through the ORAC forward model [37] for the AATSR 550 nm channel. An ocean surface with a bi-directional reflectance distribution function as described by Sayer et al. [54] which includes whitecaps, underlighting, and sun-glint was used. This model required wind and solar position. An Easterly wind with a speed of 10 m s^{-1} and solar position suitable for mid-March, when Saharan emissions are strong were selected. An effective radius of $r_{\text{eff}} = 1.62$ μm; $\tau_{550} = 1.0$ (suitable for a dust event) was used. Radiative transfer calculations used DISORT [55] to calculate the top-of-atmosphere (TOA) reflectivity, R_{TOA}.

In extreme cases (for optical properties of mineral dust that were more than 3 standard deviations from the mean values, with emission likelihoods of $< 0.1\%$) relative variation of R_{TOA} could be as large as 13% for certain viewing geometries. Within two standard deviations of the mean values (95% of all expected emissions), variations of up to 7.5% were seen. However, in terms of absolute differences in R_{TOA}, variation was below the noise limit of 2.4% for 550 nm channel [34] in all but the most extreme cases. This is shown in Fig. 6. For AATSR's nadir view (with satellite viewing angles of $\sim 0^\circ$), there are no times where the variation due to mineral dust composition is above the noise. In the forward view (with a satellite viewing angle of $\sim 55^\circ$), the variation could be above the noise for high solar angles, but this occurs at high latitudes where dust is unlikely to be seen.

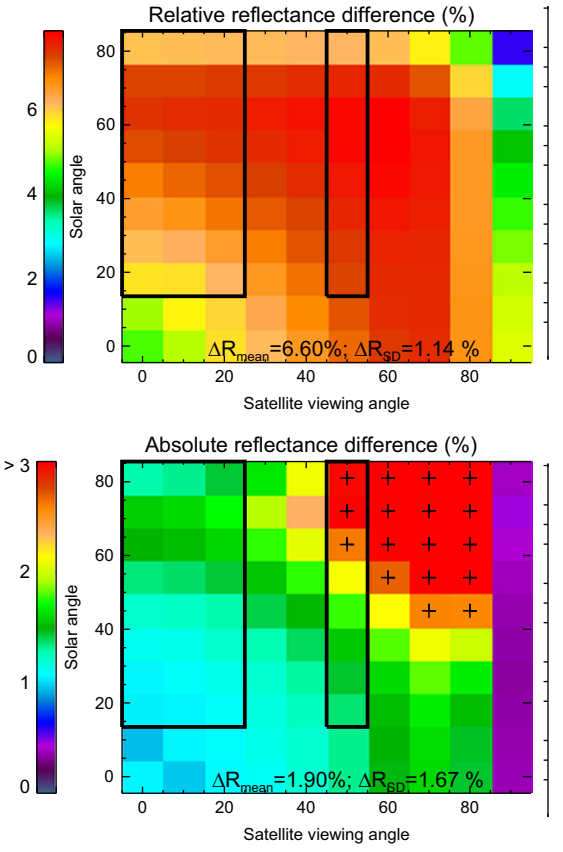

Fig. 6. Maximum variation in top-of-atmosphere reflectance at 550 nm between the mean optical properties, and a 2 SD outlier. While the maximum relative differences in reflectance can be as high as 7.5%, absolute values are generally within the AATSR noise limit of 2.4% except for certain viewing geometries (marked with a cross) where differences as large as 2.8% can occur. The areas surrounded by rectangles show the solar and satellite zenith angles where over 90% of AATSR measurements are taken.

Only one of the modelled dust types had optical properties different enough to cause significant variation above the instrument noise. This was from the Sahel, with a mean refractive index of $1.62 + 0.0033i$ but a relative emissions probability of only 0.24% and can be seen as the small red sections in Fig. 4. The high values here were due to the largest mean hematite concentrations seen: 6.5%. For composition to have any impact on the retrieval, a mean hematite content of at least 6% would be required.

Please cite this article as: Smith AJA; Grainger RG. Does variation in mineral composition alter the short-wave light scattering properties of desert dust aerosol? J Quant Spectrosc Radiat Transfer (2013), http://dx.doi.org/10.1016/j.jqsrt.2013.08.005

As discussed above, it should be noted that a size and composition independent distribution of spheroid shapes has been used to calculate individual particle light scattering properties which propagate through all radiative transfer calculations. The *AR* values used were based on SEM analysis which has a narrower range of reported asphericity than other methods of shape parameterisation. Therefore caution should be taken when assuming that changes in the composition of mineral dust has no effect on the measured optical properties.

4. Conclusions

As a result of this work, it is suggested that while the imaginary part of refractive index is very important for the correct characterisation of optical properties, particularly $\tilde{\omega}_0$, the small variations in the real part (within the range shown by the soil analysis) do not greatly affect most parts of the phase function, or the other optical properties. The variability found in k is not as large as the difference between the various values of k provided by the datasets shown in Fig. 1 and these new calculations. A 1% error in the assumed value of β^{ext} (the upper limit of differences shown here) would lead to an optical depth error of 1% which is well within the error of an aerosol retrieval. This is further shown by propagating this error through an atmospheric radiative transfer scheme, where these differences lead to variation of TOA reflectance that are (for the vast majority of cases) within the range of measurement noise.

As such, incorrect characterisation of the imaginary part of refractive index is a greater concern than the natural variability in k seen across different soil types which may be lofted into the atmosphere. Reasonable selection of the imaginary part of RI should be a high priority when considering how best to model the light scattering properties of mineral dust aerosol in visible-wavelength satellite retrievals, and should be appropriate for global use. Based on previous studies, a reasonable dust refractive index in the visible of $1.53+0.001i$ would seem appropriate.

Acknowledgements

This work was supported by the National Environmental Research Council [Grant Number NE/F007817/1].

References

[1] Kaufman YJ, Koren I, Remer LA, Tanré D, Ginoux P, Fan S. Dust transport and deposition observed from the Terra-Moderate resolution imaging spectroradiometer (MODIS) spacecraft over the Atlantic Ocean. J Geophys Res 2005;110(D10):D10S12. http://dx.doi.org/10.1029/2003JD004436.

[2] Solomon S, Qin D, Manning M, Alley R, Berntsen T, Bindoff N, et al. Climate change 2007: the physical science basis. Cambridge University Press; 2007.

[3] Ackerman SA, Cox SK. Surface weather observations of atmospheric dust over the southwest summer monsoon region. Meteorol Atmos Phys 1989;41:19–34. http://dx.doi.org/10.1007/BF01032587.

[4] Giannini A, Biasutti M, Verstraete MM. A climate model-based review of drought in the Sahel: desertification, the re-greening and climate change. Global Planet Change 2008;64(3–4):119–28, http://dx.doi.org/10.1016/j.gloplacha.2008.05.004.

[5] Jeong S-J, Ho C-H, Brown ME, Kug J-S, Piao S. Browning in desert boundaries in Asia in recent decades. J Geophys Res 2011;116(D2): D02103. http://dx.doi.org/10.1029/2010JD014633.

[6] Twomey S. Atmospheric aerosols, developments in atmospheric science, vol. 7. Elsevier Scientific Publishing Company; 1977.

[7] Washington R, Todd MC, Lizcano G, Tegen I, Flamant C, Koren I, et al. Links between topography, wind, deflation, lakes and dust: the case of the Bodélé Depression, Chad. Geophys Res Lett 2006;33: L09401. http://dx.doi.org/10.1029/2006GL025827.

[8] Sokolik IN, Toon OB. Incorporation of mineralogical composition into models of the radiative properties of mineral aerosol from UV to IR wavelengths. J Geophys Res 1999;104(D8):9423–44. http://dx.doi.org/10.1029/1998JD200048.

[9] Hess M, Koepke P, Schult I. Optical properties of aerosols and clouds: the software package OPAC. Bull Am Meteorol Soc 1998;79(5): 831–44. http://dx.doi.org/10.1175/1520-0477(1998)079⟨0831:OPOAAC⟩2.0.CO;2.

[10] Highwood EJ. Suggested refractive indices and aerosol size parameters for use in radiative effect calculations and satellite retrievals. ADIENT/APPRAISE CP2 Technical Report. Department of Meteorology, University of Reading; 2009. ⟨http://www.reading.ac.uk/adient/refractiveindices.html⟩.

[11] Claquin T, Schülz M, Balkanski YJ, Boucher O. Uncertainties in assessing radiative forcing by mineral dust. Tellus B 1998;50(5): 491–505. http://dx.doi.org/10.1034/j.1600-0889.1998.t01-2-00007.x.

[12] Remer LA, Kaufman YJ, Tanré D, Mattoo S, Chu DA, Martins JV, et al. The MODIS aerosol, algorithm products, and validation. J Atmos Sci 2005;62(4):947–73. http://dx.doi.org/10.1175/JAS3385.1.

[13] Levy RC, Remer LA, Dubovik O. Global aerosol optical properties and application to moderate resolution imaging spectroradiometer aerosol retrieval over land. J Geophys Res 2007;112(D13):D13210, http://dx.doi.org/10.1029/2006JD007815.

[14] Llewellyn-Jones D, Remedios J. The advanced along track scanning radiometer (AATSR) and its predecessors ATSR-1 and ATSR-2: an introduction to the special issue. Remote Sensing Environ 2012;116 (0):1–3. http://dx.doi.org/10.1016/j.rse.2011.06.002.

[15] Hastings DA, Emery WJ. The advanced very high resolution radiometer AVHRR: a brief reference guide. Photogramm Eng Remote Sensing 1992;58(8):1183–8.

[16] Diner DJ, Verstraete MM, Martonchik JV. Foreword to special section on MISR. IEEE Trans Geosci Remote Sensing 2002;40:1447–8, http://dx.doi.org/10.1109/TGRS.2002.802777.

[17] Levy RC, Remer LA, Tanré D, Mattoo S, Kaufman YJ. Algorithm for remote sensing of tropospheric aerosol over dark targets from MODIS. Algorithm Theoretical Basis Document MOD04/MYD04. NASA Goddard Space Flight Center; 2009.

[18] Schmetz J, Pili P, Tjemkes S, Just D, Kerkmann J, Rota S, et al. An introduction to meteosat second generation (MSG). Bull Am Meteorol Soc 2002;83(7):977–92. http://dx.doi.org/10.1175/1520-0477(2002)083<0977:AITMSG>2.3.CO;2.

[19] FAO/UNESCO. Digital soil map of the world and derived soil properties, CD-ROM; 2003. ISBN: 9789251048955.

[20] Koren I, Kaufman YJ, Washington R, Todd MC, Rudich Y, Martins JV, et al. The Bodélé depression: a single spot in the Sahara that provides most of the mineral dust to the Amazon forest. Environ Res Lett 2006;1(1):014005. http://dx.doi.org/10.1088/1748-9326/1/1/014005.

[21] Washington R, Bouet C, Cautenet G, Mackenzie E, Ashpole I, Engelstaedter S, et al. Dust as a tipping element: the Bodélé Depression, Chad. Proc Natl Acad Sci U S A 2009;106(49): 20564–71. http://dx.doi.org/10.1073/pnas.0711850106.

[22] Nickovic S, Vukovic A, Vujadinovic M, Djurdjevic V, Pejanovic G. Technical note: high-resolution mineralogical database of dust-productive soils for atmospheric dust modeling. Atmos Chem Phys 2012;12(2):845–55. http://dx.doi.org/10.5194/acp-12-845-2012.

[23] Claquin T, Schülz M, Balkanski YJ. Modeling the mineralogy of atmospheric dust sources. J Geophys Res 1999;104(D18): 22243–56. http://dx.doi.org/10.1029/1999JD900416.

[24] Laurent B, Marticorena B, Bergametti G, Leon JF, Mahowald NM. Modeling mineral dust emissions from the Sahara desert using new surface properties and soil database. J Geophys Res 2008;113: D14218. http://dx.doi.org/10.1029/2007JD009484.

[25] Sihvola A. Electromagnetic mixing formulas and applications. IEE electromagnetic waves series, vol. 47. The Institution of Electrical Engineers; 1999 ISBN 0 85296 772 1.

[26] Egan WG, Hilgeman TW. Optical properties of inhomogeneous materials: applications to geology astronomy chemistry and engineering. New York: Academic Press; 1979 ISBN 0122326504.

[27] Jacquinet-Husson N, Scott NA, Chédin A, Crépeau L, Armante R, Capelle V. The GEISA spectroscopic database: current and future

Please cite this article as: Smith AJA; Grainger RG. Does variation in mineral composition alter the short-wave light scattering properties of desert dust aerosol? J Quant Spectrosc Radiat Transfer (2013), http://dx.doi.org/10.1016/j.jqsrt.2013.08.005

archive for Earth and planetary atmosphere studies. J Quant Spectrosc Radiat Transfer 2008;109:1043–59. http://dx.doi.org/10.1016/j.jqsrt.2007.12.015.

[28] Ghosh G. Dispersion-equation coefficients for the refractive index and birefringence of calcite and quartz crystals. Opt Commun 1999;163(1–3):95–102. http://dx.doi.org/10.1016/S0030-4018(99)00091-7.

[29] Roush TL, Esposito F, Rossman GR, Colangeli L. Estimated optical constants of gypsum in the regions of weak absorptions: application of scattering theories and comparisons to independent measurements. J Geophys Res 2007;112:E10003. http://dx.doi.org/10.1029/2007JE002920.

[30] Hecht E. Optics. 4th ed.San Francisco: Addison Wesley; 2002.

[31] Marticorena B, Bergametti G, Aumont B, Callot Y, N'Doumé C, Legrand M. Modeling the atmospheric dust cycle. 2. Simulation of Saharan dust sources. J Geophys Res 1997;102(D4):4387–404, http://dx.doi.org/10.1029/96JD02964.

[32] Koren I, Kaufman YJ. Direct wind measurements of Saharan dust events from Terra and Aqua satellites. Geophys Res Lett 2004;31(6):L06122. http://dx.doi.org/10.1029/2003GL019338 ISSN 1944-8007.

[33] Alfaro SC, Gomes L. Modeling mineral aerosol production by wind erosion: emission intensities and aerosol size distributions in source areas. J Geophys Res 2001;106(D16):18075–84. http://dx.doi.org/10.1029/2000JD900339 ISSN 2156-2202.

[34] Sayer AM, Aerosol remote sensing using AATSR. PhD Thesis. Atmospheric, Oceanic and Planetary Physics, University of Oxford; 2008.

[35] Tegen I, Fung I. Contribution to the atmospheric mineral aerosol load from land surface modification. J Geophys Res 1995;100(D9):18,707–26. http://dx.doi.org/10.1029/95JD02051.

[36] Fécan F, Marticorena B, Bergametti G. Parametrization of the increase of the aeolian erosion threshold wind friction velocity due to soil moisture for arid and semi-arid areas. Ann Geophys 1999;17(1):149–57. http://dx.doi.org/10.1007/s00585-999-0149-7.

[37] Thomas GE, Carboni E, Sayer AM, Poulsen CA, Siddans R, Grainger RG. Oxford-RAL aerosol and cloud ORAC: aerosol retrievals from satellite radiometers. In: Kokhanovsky AA, de Leeuw G, editors. Satellite aerosol remote sensing over land. Springer-Praxis; 2009. p. 193–225.

[38] Buseck PR, Jacob DJ, Posfai M, Li J, Anderson JR. Minerals in the air: an environmental perspective. Int Geol Rev 2000;42(7):577–93, http://dx.doi.org/10.1080/00206810009465101 ISSN 0020-6814.

[39] Okada K, Heintzenberg J, Kai KJ, Qin Y. Shape of atmospheric mineral particles collected in three Chinese arid-regions. Geophys Res Lett 2001;28(16):3123–6. http://dx.doi.org/10.1029/2000GL012798 ISSN 0094-8276.

[40] Reid EA, Reid JS, Meier MM, Dunlap MR, Cliff SS, Broumas A, et al. Characterization of African dust transported to Puerto Rico by individual particle and size segregated bulk analysis. J Geophys Res 2003;108(D19):8591. http://dx.doi.org/10.1029/2002JD002935 ISSN 0148-0227.

[41] Kandler K, Benker N, Bundke U, Cuevas E, Ebert M, Knippertz P, et al. Chemical composition and complex refractive index of Saharan Mineral Dust at Izana, Tenerife Spain derived by electron microscopy. Atmos Environ 2007;41(37):8058–74. http://dx.doi.org/10.1016/j.atmosenv.2007.06.047 ISSN 1352-2310.

[42] Chou C, Formenti P, Maille M, Ausset P, Helas G, Harrison M, et al. Size distribution, shape, and composition of mineral dust aerosols collected during the African Monsoon Multidisciplinary Analysis Special Observation Period 0: dust and biomass-burning experiment field campaign in Niger January 2006. J Geophys Res 2008;113:D00C10. http://dx.doi.org/10.1029/2008JD009897 ISSN 0148-0227.

[43] Meland B, Kleiber PD, Grassian VH, Young MA. Correlated IR spectroscopy and visible light scattering measurements of mineral dust aerosol. J Geophys Res 2010;115(D20):20208. http://dx.doi.org/10.1029/2010JD014389 ISSN 2156-2202.

[44] Kleiber PD, Grassian VH, Young MA, Hudson PK. T-matrix studies of aerosol particle shape effects on IR resonance spectral line profiles and comparison with an experiment. J Geophys Res 2009;114:D21209. http://dx.doi.org/10.1029/2009JD012710 ISSN 2156-2202.

[45] Meland B, Alexander JM, Wong C-S, Grassian VH, Young MA, Kleiber PD. Evidence for particle size-shape correlations in the optical properties of silicate clay aerosol. J Quant Spectrosc Radiat Transfer 2012;113(7):549–58. http://dx.doi.org/10.1016/j.jqsrt.2012.01.012 ISSN 0022-4073.

[46] Veihelmann B, Volten H, van der Zande WJ. Light reflected by an atmosphere containing irregular mineral dust aerosol. Geophys Res Lett 2004;31(4):L04113. http://dx.doi.org/10.1029/2003GL018229 ISSN 1944-8007.

[47] Kahnert M, Nousiainen T, Veihelmann B. Spherical and spheroidal model particles as an error source in aerosol climate forcing and radiance computations: a case study for feldspar aerosols. J Geophys Res 2005;110:D18S13. http://dx.doi.org/10.1029/2004JD005558-ISSN 2156-2202.

[48] Dubovik O, Sinyuk A, Lapyonok T, Holben BN, Mishchenko M, Yang P, et al. Application of spheroid models to account for aerosol particle nonsphericity in remote sensing of desert dust. J Geophys Res 2006;111:D11208. http://dx.doi.org/10.1029/2005JD006619 ISSN 0148-0227.

[49] Dubovik O, Holben B, Eck TF, Smirnov A, Kaufman YJ, King MD, et al. Variability of absorption and optical properties of key aerosol types observed in worldwide locations. J Atmos Sci 2002;59(3):590–608. http://dx.doi.org/10.1175/1520-0469(2002)059⟨0590:VOAAOP⟩2.0.CO;2.

[50] Haywood JM, Francis PN, Osborne SR, Glew MD, Loeb N, Highwood EJ, et al. Radiative properties and direct radiative effect of Saharan dust measured by the C-130 aircraft during SHADE. 1. Solar spectrum. J Geophys Res 2003;108(D18):8577. http://dx.doi.org/10.1029/2002JD002687.

[51] McConnell CL, Highwood EJ, Coe H, Formenti P, Anderson B, Osborne S, et al. Seasonal variations of the physical and optical characteristics of Saharan dust: results from the dust outflow and deposition to the ocean experiment. J Geophys Res 2008;113:D14S05, http://dx.doi.org/10.1029/2007JD009606.

[52] McConnell CL, Formenti P, Highwood EJ, Harrison MAJ. Using aircraft measurements to determine the refractive index of Saharan dust during the DODO Experiments. Atmos Chem Phys 2010;10(6):3081–98. http://dx.doi.org/10.5194/acp-10-3081-2010.

[53] Shi Z, Krom MD, Bonneville S, Baker AR, Bristow C, Drake N, et al. Influence of chemical weathering and aging of iron oxides on the potential iron solubility of Saharan dust during simulated atmospheric processing. Global Biogeochem Cycles 2011;25(2):GB2010. http://dx.doi.org/10.1029/2010GB003837.

[54] Sayer AM, Thomas GE, Grainger RG. A sea surface reflectance model for (A) ATSR, and application to aerosol retrievals. Atmos Meas Tech 2010;3(4):813–38. http://dx.doi.org/10.5194/amt-3-813-2010.

[55] Stamnes K, Tsay S-C, Wiscombe W, Jayaweera K. Numerically stable algorithm for discrete-ordinate-method radiative transfer in multiple scattering and emitting layered media. Appl Opt 1988;27(12):2502–9. http://dx.doi.org/10.1364/AO.27.002502.

Please cite this article as: Smith AJA; Grainger RG. Does variation in mineral composition alter the short-wave light scattering properties of desert dust aerosol? J Quant Spectrosc Radiat Transfer (2013), http://dx.doi.org/10.1016/j.jqsrt.2013.08.005